Dalton Transactions

ARTICLE

Synthesis, Structure and Photophysical Properties of a 2D Network with Gold Dicyanide Donors Coordinated to Aza[5]helicene Viologen Acceptors

Received 00th January 20xx,
Accepted 00th January 20xx

DOI: 10.1039/x0xx00000x

www.rsc.org/

Ealin N. Patel,[a] Robert B. Arthur,[a] Aaron D. Nicholas,[a] Eric W. Reinheimer,[b,c] Mohammad A. Omary,[c] Matthew Brichacek,[a*] and Howard H. Patterson[a*]

A recently synthesized photoluminescent organic acceptor, 5,10-dimethyl-5,10-diaza[5]helicene is shown to react with dicyanoaurate anions to form a 2D network N,N-Dimethylaza[5]helicene dicyanoaurate. The structure of the synthesized complex was investigated via X-ray crystallography showing the presence of $[Au(CN)_2]^-$ dimers and monomers within the helicene framework. Photophysical measurements between 298 K and 10 K indicate quenching of the $[Au(CN)_2]^-$ anion by 5,10-dimethyl-5,10-diaza[5]helicene via an electron transfer. A Stern-Volmer and Rehm-Weller analysis shows that this is a result of quenching from transfer of an electron from $[Au(CN)_2]^-$ anions to 5,10-dimethyl-5,10-diaza[5]helicene as opposed to resonance energy transfer. DFT calculations were performed to support the assignment of an electron transfer.

Introduction

Viologens are redox active, strong electron accepting diquaternary salts of 4,4'-bipyridine with the ability to form ion-pair charge transfer complexes (IPCT) with donors such as dicyanoaurate. Charge transfer properties of IPCT can be applied in photochromic and electrochromic devices.[1–4] The photoreduction properties of viologens have been known for several years with applications as herbicides, photocleaving agents, and electronic devices. However, the photophysical and photochemical properties of viologens are mostly unexplored.[5] Phenyl-viologens such as 1,1'-bis-(2,4-dinitrophenyl)-4,4'-bipyridinium (DNP^{2+}) have shown desirable optical and electronic properties due to extended π conjugation.[6,7] The π-π stacking interactions of phenyl viologens are being explored in chemistry and biology due to its effect on the photophysical properties of 2D and 3D networks.[8] In conjunction, dicyanoaurate (I) complexes are also of interest as they form one of the most stable two-coordinate complexes, with reports of high stability constants as well as potential applications in semiconductor materials and photonic devices.[9,10] Dicyanoaurate(I) has also unique geometric and charge-transfer properties as the d^{10} Au(I) metal center favors aurophilic interactions and aggregation of $[Au(CN)_2^-]^{n-}$, which allow tuning of the optical properties.[7,11]

Due to their strong electron accepting potential, viologens are luminescence quenchers of triplet metal-to-ligand charge transfer (MLCT) luminescence in complexes containing Au(I). In our previous studies, we observed low energy phosphorescence from a 3D network consisting of DNP^{2+} coupled with dicyanoaurate(I) dimers (**Fig.1**).[7] These results were surprising given that DNP^{2+} is non-luminescent in its free state. The observed luminescence in this complex revealed unique photophysical properties that were attributed to an IPCT transition arising from the heavy atom effect due to gold-viologen orbital overlap.[7,12] It would be interesting to study the photochemical interaction of other methylated phenyl viologens which possess extended π conjugation and are luminescent in the free state with dicyanoaurate(I). 5,10-dimethyl-5,10-diaza[5]helicene bistetrafluoroborate viologen was synthesized a few years ago and the synthetic route has recently been optimized.[5,12] In addition, it is one of the few viologens known which has chirality due to the helical aromatic heterocycle.[5,13] It was shown that this compound has energy holding abilities and is a good electron transfer contender due to its V_e being greater than V_h (electronic coupling for electron and hole respectively).[14] The conductivity spectra and refractive index of this viologen highlighted its ability of high intra/inter molecular charge transfer within the crystal and ability to yield significant outputs with low input.

In our current study, we extend our previous work on methyl viologen (MV^{+2}) systems by synthesizing 5,10-dimethyl-5,10-diaza[5]helicene (heli[5]viologen ($\mathbf{7}^{2+}$) and coupling it with two molecules of $[Au(CN)_2]^-$ to form complex **8** as shown in **Fig. 1**. We report the synthesis and characterization of the N,N-dimethylaza[5]helicene dicyanoaurate (Au heli-viologen) complex using nuclear magnetic resonance (NMR). The crystal structure of Au heli-viologen was determined by single crystal X-ray diffraction. We studied the optical properties of this complex using temperature variable photoluminescence, diffuse

[a] Department of Chemistry, University of Maine, Orono, ME 04469.
[b] Department of Chemistry and Biochemistry and the W.M. Keck Foundation Center for Molecular Structure, California State University, San Marcos, CA 92096.
[c] Department of Chemistry, University of North Texas, Denton, TX, 76203
Electronic Supplementary Information (ESI) available: [details of any supplementary information available should be included here]. See DOI: 10.1039/x0xx00000x

reflectance spectroscopy (DRS), and Stern-Volmer analysis. Density Functional Theory (DFT) calculations were performed to assist with interpretation of the experimental data.

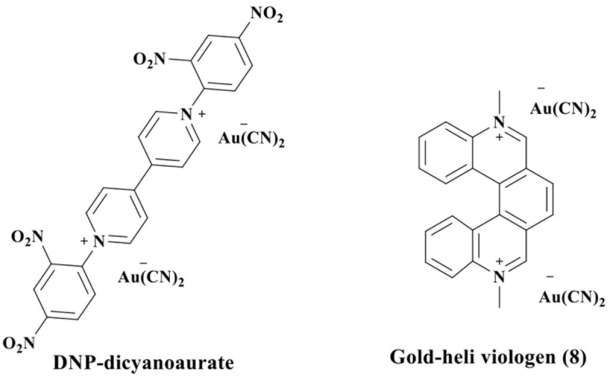

Fig. 1. Previously studied DNP^{2+} viologen complex with dicyanoaurate and complex **8**, Au heli-viologen (5,10-diazadimethyl[5]helicene viologen complexed with dicyanoaurate)

Experimental

Synthetic procedures.

General procedure. All reagents were purchased from Sigma-Aldrich and Fisher Scientific and used directly without further purification. All products were purified with silica-gel flash chromatography or preparative HPLC. HPLC was performed on a Gilson analytical to semi-preparative system using Kinetex 5 µm EVO C18 100Å 4.6 x 150 mm for analytical and Kinetex 5 µm EVO C18 100Å 21.1 x 150 mm for preparative purpose. Products were characterized by ^{1}H and ^{13}C NMR and mass spectrometry. NMR characterization results and *J* values were compared with published results. ^{1}H and ^{13}C NMR spectra were recorded on Agilent/Varian 400 MHz and 101 MHz NMR spectrometer respectively. Mass spectra were recorded using a Synapt G2 Q-TOF ESI mass spectrometer. Mass spectra for all reported compounds can be found in the ESI.

Synthesis of bis-1,2-tributylstannyl ethylene (2). Tributylstannyl acetylene (328 mg, 1 mmol) & tributylstannyl hydride (291 mg, 1 mmol) were added to a vial with AIBN (3.3 mg, 0.02 mmol). The mixture was heated and stirred at 100 ºC for 6 hrs. Water was added to the reaction mixture and the product was extracted with four aliquots of methylene chloride and dried over Na_2SO_4. The solvent was evaporated under reduced pressure yielding **2**. This product was used in the following step without further purification. Yield: 549 mg (90%). **^{1}H NMR (400 MHz, $CDCl_3$)** δ 6.89 (s, 2H), 1.46-1.64 (m, 12H), 1.25-1.44 (m, 12H), 0.80-0.98 (m, 30H) ppm.

Synthesis of (E)-1,2-di(quinoline-3-yl)ethene (4).

Stille Coupling. 3-Bromoquinoline (**1**) (131 mg,0.63 mmol) and compound **2** (194 mg, 0.32 mmol) were added to a vial purged with N_2. Tris(dibenzylideneacetone)dipalladium (Pd(0) catalyst, 5 mol%) & 2-dicyclohexylphosphino-2',4',6'-triisopropylbiphenyl (Xphos, 0.2 eq.) were added to the reaction vial, followed by addition of dry toluene (4 mL) under N_2. The reaction mixture was heated at 110 ºC for 2 days. The solvent was evaporated under reduced pressure and the crude product was purified with flash chromatography using 70%:30% ethyl acetate:hexane mixture with 1% triethylamine to get (E)-1,2-Di(quinoline-3-yl)ethene. Yield: 51 mg (57%).

Hiyama-Heck Coupling. A mixture of triethoxyvinylsilane **(3)** (0.43 g, 2.25 mmol) and sodium hydroxide (0.5 M, 18 mL) was added to a 40 mL pressure vial, followed by addition of 3-bromoquinoline (**1**) (0.75 g, 3.60 mmol) & palladium acetate (0.5 mol%). The reaction vial was sealed with a heat resistant teflon resistant screw cap and the mixture was stirred at 140 ºC for 6 hrs. After cooling, the green precipitate was filtered and washed with 10:1 ethyl acetate:chloroform. The solvent was evaporated under vacuum. Yield: 0.46 g (91%). **^{1}H NMR (400 MHz, $CDCl_3$)** δ 9.19 (d, 2H, *J*=2.1 Hz), 8.25 (d, 2H, *J*=2.1 Hz), 8.11 (d, 2H, *J*=8.4 Hz), 7.86 (d, 2H, *J*=8.0 Hz), 7.72 (ddd, 2H, *J*=8.3,7.0,0.9 Hz), 7.58 (ddd, 2H, *J*=8.1, 6.7, 0.9 Hz), 7.47 (s, 2H) ppm. **^{13}C NMR (101 MHz, DMSO-d^6)** δ 175.40, 151.16,149.62,145.85, 137.60, 130.34, 130.07, 128.96, 127.61, 116.79 ppm. **HRMS (TOF MS ES+)** m/z calculated for $C_{20}H_{15}N_2$ ($[M-H]^+$) 283.1235, found 283.1231

Synthesis of 5,10-diaza[5]helicene (5). Compound **4** (0.6 g, 2.1 mmol) was dissolved in ethyl acetate (500 mL) in a round bottom flask. A condenser was attached to the top and the setup was mounted inside an RPR-100 photoreactor on a stir-plate. The mixture was stirred and irradiated at 350 nm for 7 hrs. The crude product was purified with silica-gel chromatography using 70%:30% ethyl acetate:hexane. Yield: 0.43 g (73%). **^{1}H NMR (400 MHz, $CDCl_3$)** δ 9.46 (s, 2H), 8.65 (dd, 2H, *J*=8.4, 1.2 Hz), 8.29 (dd, 2H, *J*=8.3, 1.3 Hz), 8.14 (s, 2H), 7.76 (ddd, 2H, *J*=8.3, 7.0, 1.3 Hz), 7.44 (ddd, 2H, *J*=8.4, 7.0, 1.3 Hz) ppm. **^{13}C NMR (101 MHz, $CDCl_3$)** δ 152.53, 145.88, 129.71, 129.48, 129.43, 128.17, 127.32, 127.26, 125.61, 124.38 ppm. **HRMS (TOF MS ES+)** m/z calculated for $C_{20}H_{13}N_2$ ($[M-H]^+$) 281.1079, found 281.1070. Benzo-[b]-1,8-diaza[4]-helicene (**6**) was recovered as a side-product. Yield: 0.11 g (19%) (ESI)

Synthesis of dimethylaza[5]helicene (7) (bis-tetrafluoroborate-7a or dichloride salt-7b). To trimethyl oxonium tetrafluoroborate (Meerwein's salt, 0.356 g, 2.39 mmol) in a 40 mL scintillation vial was added anhydrous methylene chloride (100 mL) under N_2. 5,10-diaza[5]helicene (**5**) (0.223 g, 0.80 mmol) in anhydrous methylene chloride (20 mL) was then added to the vial under N_2. The vial was stirred under N_2 for 24 hrs. Methylene chloride was removed under vacuum. The dried yellow solid was triturated with warm 90% ethanol. The crude (**7a)** was further purified with preparative HPLC using 5% to 15% acetonitrile in 10 minutes. Yield: 233 mg (60%). DOWEX 1×8 200-400 mesh ion-exchange resin (*Acros)* (11.25 g) was loaded onto a column and washed with methanol followed by equilibration with 50% aqueous ethanol. Compound **7a** (225 mg, 0.46 mmol) dissolved in acetonitrile (0.5 mL) was loaded into the column. The column was washed with 50% aqueous ethanol. The fractions were concentrated and reloaded on the column and collected two more times. Combined fractions were concentrated under reduced pressure to yield the product (**7b**). Yield: 167 mg (95%).

***7a*- ^{1}H NMR (400 MHz, CD_3CN)** δ 10.04 (d, 2H, *J*=2.2 Hz), 8.72 (d, 2H, *J*=8.5 Hz), 8.67 (d, 2H, *J*=1.5 Hz), 8.57 (d, 2H, *J*=8.5

Hz), 8.24 (ddd, 2H, *J*=8.7, 7.4, 1.3 Hz), 7.88 (ddd, 2H, *J*=8.3, 7.3, 1.0 Hz), 4.82 (s, 6H) ppm. **^{13}C NMR (101 MHz, CD_3CN)** δ 154.82, 136.93, 135.12, 133.74, 131.78, 131.06, 129.86, 129.32, 127.33, 120.34, 47.60 ppm. **HRMS (TOF MS ES+)** m/z calculated for $C_{20}H_{15}N_2$ ($[M]^{+2}$) 155.0735, found 155.0731

***7b*-^{1}H NMR (400 MHz, CD_3OD)** δ 10.54 (d, 2H, *J*=2.2 Hz), 8.86 (d, 2H, *J*=8.4 Hz), 8.82 (d, 2H, *J*=1.2 Hz), 8.75 (d, 2H, *J*=8.7 Hz), 8.28 (ddd, 2H, *J*=8.6, 7.3, 1.3 Hz), 7.92 (ddd, 2H, *J*=8.2, 7.3, 1.0 Hz), 4.99 (s, 6H) ppm. **^{13}C NMR (101 MHz, CD_3OD)** δ 155.89, 137.21, 135.33, 133.99, 132.12, 130.97, 130.46, 129.73, 127.63, 120.59, 47.12 ppm. **HRMS (TOF MS ES+)** m/z calculated for $C_{20}H_{15}N_2$ ($[M]^{+2}$) 155.0735, found 155.0735

Synthesis of Au heli-viologen (8). To a solution of N,N-Dimethylaza[5]helicene dichloride (**7b**) (40 mg, 0.104 mmol) in water (30 mL), potassium dicyanoaurate (60 mg,0.21 mmol) in water was added while stirring. The precipitate was filtered after 10-12 hours and solvent was slowly evaporated to complete the precipitation of N,N-Dimethylaza[5]helicene dicyanoaurate (**8**). Yellow solid was dried under reduced pressure and used for crystallization. Yield- 49 mg (58%).

Crystallization. Au heli-viologen (Complex **8)** (10 mg) was dissolved in ethanol (0.2 mL) in a 2 mL scintillation vial. This vial was covered with porous aluminum foil and placed in a 20 mL scintillation vial containing cyclohexane (2 mL). This closed system was kept inside the fume hood for 8 to 9 days. Small crystals formed through slow vapor diffusion. Results were reproduced with methanol as a solvent and n-hexane as anti-solvent.[15]

^{1}H NMR (400 MHz, CD_3OD) δ 10.49 (d, 2H, *J*=2.2 Hz), 8.89 (d, 2H, *J*=8.8 Hz), 8.80 (d, 2H, *J*=2.1 Hz), 8.75 (d, 2H, *J*=9.0 Hz), 8.29 (ddd, 2H, *J*=8.6, 7.5, 1.1 Hz), 7.95 (ddd, 2H, *J*=8.6, 7.5, 1.1 Hz), 4.97 (s, 6H) ppm. **^{13}C NMR (101 MHz, D_2O)** δ 153.67, 135.70, 134.10, 133.08, 130.69, 129.96, 129.93, 128.96, 128.51, 126.43, 119.03 ppm.

Crystallography. A small yellow block-like crystal of Au heli-viologen (**8**) having dimensions 0.057 x 0.063 x 0.092 mm^3 was secured to a Mitegen cryomount using Paratone oil. Single crystal reflection data were collected on a Rigaku Oxford Diffraction (ROD) Synergy-S X-ray diffractometer equipped with a HyPix-6000HE hybrid photon counting (HPC) detector. The data were collected at 100 K using Mo $K_{\alpha1}$ radiation from a data collection strategy calculated using CrysAlis^{Pro} which was also responsible for unit cell determination, initial indexing, data collection, frame integration, Lorentz-polarization corrections and final cell parameter calculations.[16] A numerical absorption correction via face indexing was performed using the SCALE3 ABSPACK algorithm integrated into CrysAlis^{Pro}.[17] The crystal structure was solved via intrinsic phasing using ShelXT and refined using *olex2.refine* within the Olex2 graphical user interface.[18–20] The structural model's space group was unambiguously verified by PLATON.[21] Structural refinement of the reflection data for **8** resulted in the identification of electron density peaks associated with a highly disordered interstitial CH_2Cl_2 molecule that could not be satisfactorily modeled. This minor impurity may have been trapped during screening of solvents for crystallozation. The data were treated using the SQUEEZE routine in PLATON, then refined on F^2 to acceptable levels.[22] The final structural refinement included anisotropic temperature factors on all non-hydrogen atoms and hydrogen atoms were attached via the riding model at calculated positions using appropriate HFIX commands. The crystallographic and refinement data for Au heli-viologen is listed in **Table 1**. Crystallographic data for this paper has been deposited with the Cambridge Crystallographic Data Centre with the CCDC number 1558366. This data can be obtained free of charge from the Cambridge Crystallographic Data Centre via www.ccdc.cam.ac.uk/data_request/cif.

Spectroscopy studies. Steady-state photoluminescence scans were collected between 298 K and 10 K. Spectra were taken with a Model Quantamaster-1046 photoluminescence spectrophotometer from Photon Technology International using a 75 W xenon arc lamp combined with two excitation monochromators and one emission monochromator. A photomultiplier tube at 800 V was used as the emission detector. The solid samples were mounted on a copper plate using non-emitting copper-dust high vacuum grease. All scans were collected under vacuum with a Janis ST-100 optical cryostat. Infrared spectra were collected on solid samples at 298 K using a Perkin Elmer FT-IR Spectrum Two equipped with a Universal Attenuated Total Reflectance (UATR) accessory and a LiTaO3 MIR detector. Diffuse reflectance spectra were collected on solid samples at 298 K. The light source was a Mikropack DH-2000 deuterium and halogen light source coupled with an Ocean Optics USB4000 detector. Scattered light was collected with a fiber optic cable. Spectra was referenced with polytetrafluoroethylene. Data was processed using SpectraSuite 1.4.2_09.

Stern-Volmer quenching experiments. For quenching experiments, $\mathbf{7}^{2+}$ was used as the quencher. After determining proper quencher concentration ranges, the quenching experiment performed using the $[Au(CN)_2]^-$ sample solutions. A stock solution of 5 x 10^{-4} M $K[Au(CN)_2]$ was first prepared, and then 1 mL of stock solution was distributed among all quenching vials. The quencher solution was then added to the quenching vials in increments of 50 uL. The contents of each vial were then transferred to cuvettes and the emission spectrum of each sample was measured separately. Emission scans were conducted on a Jobin Yvon Systems Fluorolog 3 Spectrofluorometer. The excitation monochromator was referenced to a secondary detector, and the emission monochromator was calibrated to a water Raman peak to ensure the accuracy of scans.

Molecular modelling. All geometry parameters were determined using Gaussian '16 software (Gaussian Inc.) with the University of Maine Advanced Computing Group.[23] All ground state and excited state calculations were performed using density functional theory (DFT) and time-dependent density functional theory (TD-DFT) calculations using the M06 meta-hybrid functional[24,25] with the CEP-31G(d) basis set employed for all atoms.[26,27] XRD structures were used as initial structural input. From the structural data we have developed a neutral model that is composed of two $\mathbf{7}^{2+}$ units bridged by a dimer $[Au(CN)_2]_2^{-2}$ and capped with terminal $[Au(CN)_2]^-$ monomer units. This model contains all subunits present within the crystal structure. Isodensity representations of molecular orbitals were generated using GaussView 5.0 software (Gaussian Inc.). MOs were generated and visualized using the Avogadro 1.2.0 software program.[28]

Results and discussion

Synthesis. In order to access the Au heli-viologen (**8**), two different salts of $\mathbf{7}^{2+}$ were made as shown in **Scheme 1**. Initially, a stepwise synthetic route was used to access compound **4** via a Wittig reaction in four steps from quinoline-3-carbaldehyde.[13] A palladium catalyzed route was eventually preferred over the stepwise route to increase efficiency and yield. Stille coupling with 3-bromoquinoline and **2** using Pd(0) catalyst and Xphos ligand produced relatively low yield (57%) of the desired compound **4**. Pd(II) catalyzed Hiyama-Heck cross-coupling was explored with triethoxyvinylsilane to get better scalability and higher yield (91%).[5]

5,10-diaza[5]helicene (**5**) was made by photocyclization of **4** in a photoreactor (350 nm), which was equipped with a magnetic stir plate, and cooling fan to minimize the heating. Methylation of **5** with trimethyloxonium tetrafluoroborate under nitrogen produced the BF_4 salt of heli[5]viologen (**7a**) which was purified with preparative HPLC. Due to the limited solubility of **7a** in aqueous solvents, the tetrafluoroborate counterion was exchanged for chloride counterions using DOWEX ion-exchange resin. The chloride heli-viologen (**7b**) showed high solubility in aqueous solvents and was further reacted with potassium dicyanoaurate to produce gold-coupled viologen, **8** in powder form. The powder was dried and used for luminescence experiments and crystallization via vapor diffusion method. The crystallization conditions via a vapor diffusion method for Au heli-viologen (**8**) were optimized and methanol:n-hexane and ethanol:cyclohexane were used as solvent:anti-solvent to get single crystals for X-ray diffraction analysis.[15]

Scheme 1. Overall synthetic scheme.

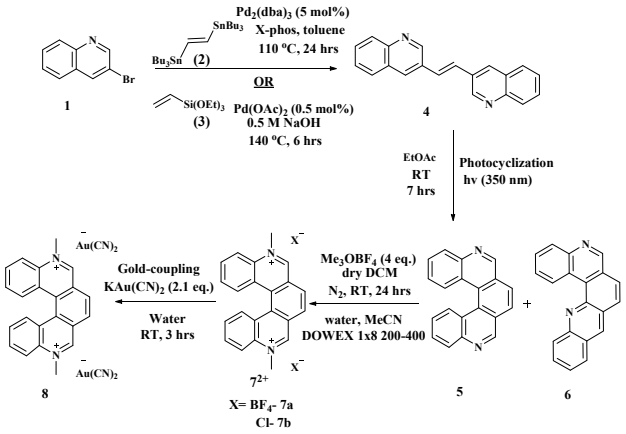

Single Crystal X-Ray Diffraction. The solid state structure of Au heli-viologen crystallized in the centrosymmetric monoclinic space group *C2/c* and contained one viologen dication and two $[Au(CN)_2]^-$ anions on general positions as the elements of the asymmetric unit (**Fig. 2**). When looking into the *bc*-plane of the unit cell, one of the $[Au(CN)_2]^-$ anions lies perpendicular to this plane (and parallel to the *a*-axis) at a distance of 3.3773(6) Å between the Au(I) atom of the dicyanoaurate anion and the centroid of the aromatic ring sitting at the turn of the right-handed helical viologen. Typically, dicyanoaurate anions are linear with N-Au-N angles approaching 180°; however within the structure of Au heli-viologen, the $[Au(CN)_2]^-$ anion lying above the turn of the helicate deviates from linearity, showing an N-Au-N angle of 174.0(3)°.[29] Such a deviation from linearity can be

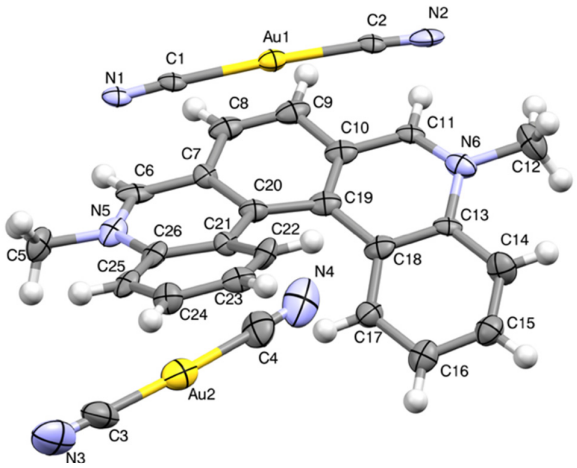

Fig. 2. Asymmetric unit elements of Au heli-viologen containing a viologen dication and two $[Au(CN)_2]^-$ anions. Ellipsoids shown at 50% probability.

rationalized upon the application of symmetry to the asymmetric unit. After applying crystallographic symmetry, this dicyanoaurate anion dimerizes with itself and supports the formation of a bond between the monovalent gold atoms at a distance of 3.3098(11) Å, a value on par with those published in a previous report.[30] As a direct consequence of the binding of the neighboring, symmetry-equivalent $[Au(CN)_2]^-$ anions to one another, their dimerization imparts some structural rigidity as evidenced by the smaller size of the thermal parameters of the dimer's constituent gold, carbon and nitrogen atoms.

Projections of the asymmetric unit along the *b*-axis (**Fig. 3**) demonstrated strong one-dimensional overlap between the dimerized $[Au(CN)_2]^-$ anions and the nearly-planar region of the viologen dications parallel to that axis. Such an orientation of these moieties relative to one another within the solid state structure may provide evidence for the onset of interesting spectroscopic properties. Despite the potential for the dicyanoaurate anion located above the turn of the helical viologen in concert with its propensity to dimerize upon the application of crystallographic symmetry to generate interesting spectroscopic features, the second $[Au(CN)_2]^-$ anion in the asymmetric unit does not dimerize upon the application of crystallographic symmetry. Unlike the anion in the asymmetric unit which does dimerize, the second anion has much more linear geometry as evidenced by its N-Au-N angle of 176.5(5)°. Thermal parameters for the second dicyanoaurate anion also demonstrate more thermal motion as evidenced by the larger anisotropic displacement ellipsoids for its constituent gold, carbon and nitrogen atoms. Between the anion and the helical viologen, the closest contact occurred between the centroid of the phenyl at the turn in the helix and N4 from the terminal nitrile at a distance of 3.351(19) Å. This distance suggests the onset of a potential dipole-dipole interaction given the positioning of the electron-rich nitrile relative to the electron-deficient phenyl ring of the dication.[31] Also, given the less intimate molecular orbital overlap between this latter dicyanoaurate and the planar surface of the viologen, suggests that unlike the former $[Au(CN)_2]^-$, the latter is more spectroscopically innocent. As a consequence, Au heli-viologen can be described as a 2D network consisting of a series of noninteracting stacked $[Au(CN)_2]_2^{-2}/\mathbf{7}^{2+}$ slabs.

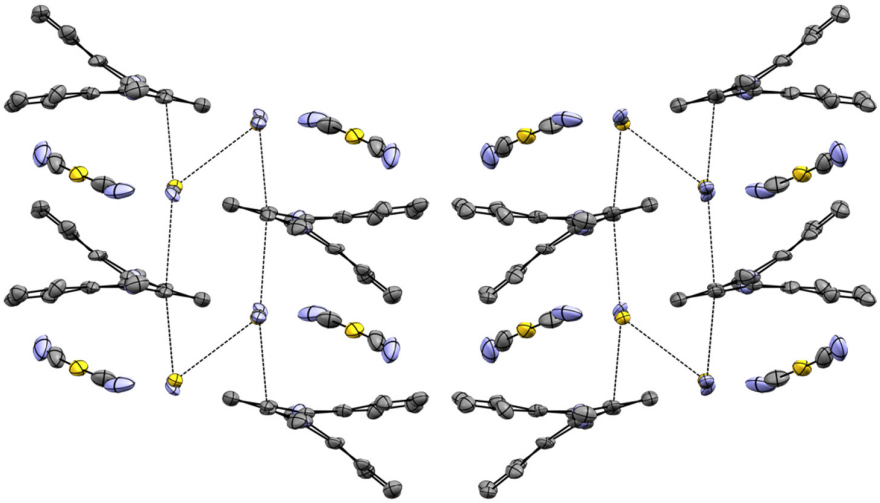

Fig. 3. View along the *a*-axis of Au heli-viologen crystal. The dotted lines show dimer interactions among adjacent $[Au(CN)_2]^-$ anions and helicenes.

Compound	**Au heli-viologen**
CCDC Code	1558366
Formula	C26H18Au2N6
Formula weight	808.41
Temp.	100(2)
Space group	C2/c
a, Å	13.7875(4)
b, Å	12.4750(3)
c, Å	28.7102(8)
α, deg	90.00
β, deg	91.977(3)
γ, deg	90.00
volume, $Å^3$	4935.2(2)
Z	8
Density (calculated), mg/m^3	2.176
μ, mm^{-1}	11.903
Scan	ω scan
ϑ range for data collection, deg	6.68-50.06
Reflections measured	4339
Independent observed reflns.	4338
Independent reflns. [$I>2\sigma$]	4082
Data/restraints/parameters	4338/38/273
R_{int}	0.0244
Final *R* Indices [$I>2\sigma$]	$R_1 = 0.0593$, $wR_2 = 0.1471$
R Indices (all data)	$R_1 = 0.0620$, $wR_2 = 0.1481$
Goodness-of-fit on F^2	1.009

[a] $R = R_1 = \sum|F_o|-|F_c||/\sum|F_o|$ for observed data only. $R_w = wR_2 = \{\sum [w(F_o^2 - F_c^2)^2]/ \sum [w(F_o^2)^2]\}^{1/2}$ for all data.

Table 1. Crystal refinement data of Au heli-viologen. Select bond lengths and angles available in Table S1 and S2 (ESI).[a]

Analysis of the bond distances within the different $[Au(CN)_2]^-$ anions as a function of their being free or dimerized in the solid state also revealed subtle differences (**Fig. 3**). Within the dicyanoaurate anion that dimerizes, the bond distances between the nitriles and the Au(I) were measured at distances of 2.007(16) and 2.011(15) Å while those in the free anion were measured at 1.98(2) and 1.94(2) Å respectively. The nitrile distances from the different anions also revealed differences as those from the dimerized anion were measured at 1.09(2) and 1.132(19) Å while their analogues from the free $[Au(CN)_2]^-$ revealed distances of 1.12(3) and 1.17(3) Å between the constituent carbon and nitrogen atoms. Such a difference can be hypothesized on the basis of dimerization between the neighboring dicaynoaurate anions upon the application of symmetry. Electron density is donated from the nitrile into the corresponding Au-C bond, resulting in a shortening of the former and a lengthening of the latter. This build-up of electron density on the monovalent Au atom, in concert with the nearby positioning of a symmetry-related anion, supports bond formation between the gold atoms. Relevant bond distances within the free dicyanoaurate anion are similar to those reported in the literature as no intramolecular donation of electron density to support Au-Au bond formation occurs.[29]

Infrared Spectroscopy. Au heli-viologen (**8**) is a coordination polymer, where a dominant vibrational feature is the cyanide stretch. We show the IR vibrational spectra of this region in **Fig. S13** (ESI). The ν_s(C≡N) of the gold(I) dicyanide anions are observed at 2,140 cm^{-1}, 2,152 cm^{-1}, 2,160 cm^{-1}, and 2,165 cm^{-1}, indicating that the CN ligands are slightly inequivalent throughout the crystal motif. This split is in agreement with the structural data which shows the presence of monomer $[Au(CN)_2]^-$ and dimer $[Au(CN)_2]_2^{-2}$ units. For oligomer units of metal cyanides, the ν_s(C≡N) vibrational mode moves to lower energies as the oligomer size increases due to the increased electron density of the CN π^* LUMO.[32] In keeping with this, we have assigned the bands at 2,140 cm^{-1} and 2,152 cm^{-1} to the ν_s(C≡N) vibration modes of the dimers and the 2,160 cm^{-1} and 2,165 cm^{-1} bands to the vibrational modes of the monomer subunits.

Photophysical Studies. To investigate the absorption of Au heli-viologen, we have performed diffuse reflectance measurements of solid microcrystalline samples of both Au heli-viologen (**8**) and $\mathbf{7}^{2+}$ at 298 K (**Fig. 4**). Solid samples of gold coordinated $\mathbf{7}^{2+}$ are yellow in color and absorb strongly in the UV. As seen in the spectra, the absorption falls off sharply around 475 nm with an optical absorption edge of 2.39 eV. This edge is slightly more variable for the gold free $\mathbf{7}^{2+}$ which slowly tappers off through the visible range and is identical to previous reports of MV^{2+} which are assigned to a $\pi\rightarrow\pi^*$ state.[5] Introduction of $[Au(CN)_2]^-$ results in few changes in the DRS spectra in comparison to $\mathbf{7}^{2+}$. The appearance of higher energy bands at 268 nm not observed in the gold free $\mathbf{7}^{2+}$ are assigned to a metal to ligand charge transfer (MLCT) localized to the $[Au(CN)_2]^-/[Au(CN)_2]_2^{-2}$ subunits consistent with reports elsewhere.[33] The majority of the band remains a $\pi\rightarrow\pi^*$ state of the $\mathbf{7}^{2+}$.

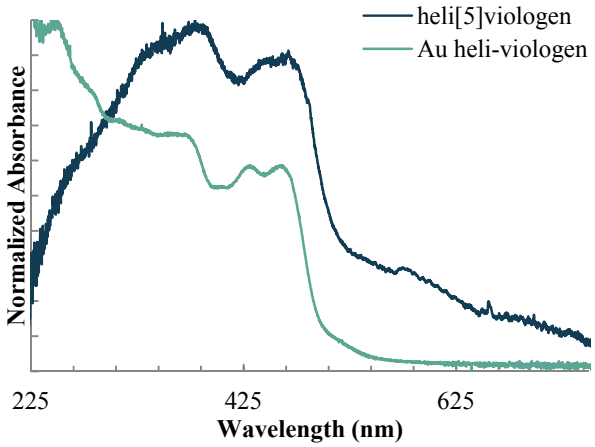

Fig. 4. Solid state DRS absorption spectrum of solid samples of Au heli-viologen and MV^{2+} at 298 K converted via Kubelka-Monk.

As an aromatic cation, $\mathbf{7}^{2+}$ is well equipped to accept electrons from the electron rich gold(I) dicyanide anions as reported for other viologen like molecules.[7] To probe this we have performed temperature variable photoluminescence measurements of microcrystalline samples of Au heli-viologen between 298 K and 10 K. The spectra are shown in **Fig. 5** and are overlaid to demonstrate the change in peak shape and relative intensity with respect to temperature. We observe that the excitation spectrum of Au heli-viologen (**8**) consists of two bands: one high energy band at 375 nm, and one low energy band at 470 nm. A shift in the relative intensity towards the high energy band is observed upon temperature change. No significant shift in the position of either excitation band is observed at lower temperatures. At room temperature, compound **8** in microcrystalline form shows one broad triplet emission band at 580 nm ($\tau_{298\ K}$ = 1.01 μs, $\tau_{78\ K}$ = 1.12 μs). At lower temperatures the relative emission intensity increases and a second, lower-energy band appears at 608 nm. This band first appears at 129 K, and does not shift during cooling. Time-dependent measurements show much shorter lifetime of this band ($\tau_{78\ K}$ = 130 ns) in comparison to that of the band at 580 nm. Based on previous reports of $\mathbf{7}^{2+}$ the data reported here, the 580 nm band is assigned to a triplet $\pi\rightarrow\pi^*$ localized to $\mathbf{7}^{2+}$. The emission band observed at 608 nm is a new feature and was not observed in previous reports of 7^{2+}. Both the lifetime and wavelength of this band are too long for cation $S_1\rightarrow S_0$ emission. Instead these values better fit expected values for $[Au(CN)_2]^-$ emission. We have observed similar behavior in $Au(CN)_2^-/DNP^{+2}$ structures where low temperature emission is dominated by $[Au(CN)_2]^-$ bands but quenched at 298 K.[7] The absence of $[Au(CN)_2]^-$ emission above 129 K indicates quenching by $\mathbf{7}^{2+}$ at high temperatures. In this case we believe an oxidative electron transfer in the excited state at higher temperatures between $[Au(CN)_2]^-$ and $\mathbf{7}^{2+}$ occurs (**Fig. 6**).

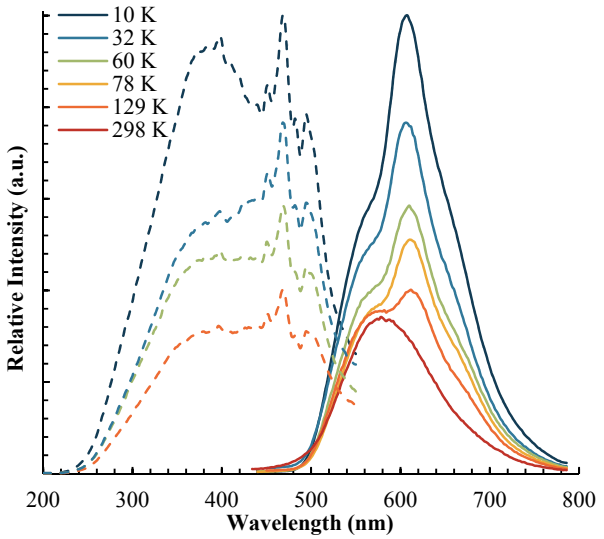

Fig. 5. Luminescence spectra of Au heli-viologen between 10 K and 298 K. Excitation (dashed) and emission (solid).

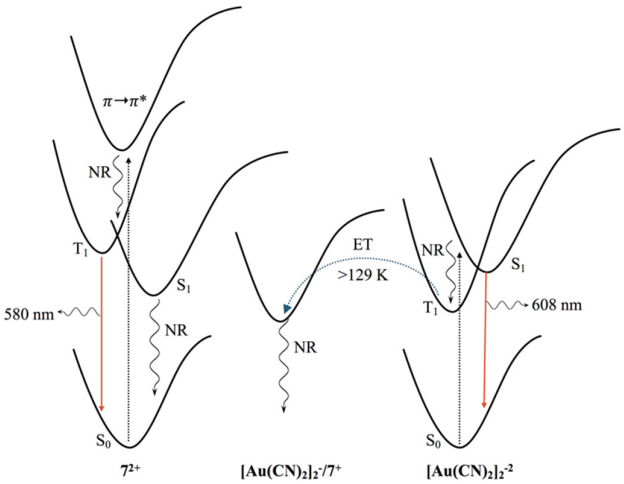

Fig. 6. Energy diagram of emission pathways for Au heli-viologen. At higher temperatures the 7^{2+} emission by $T_1\rightarrow S_0$ is favored along with quenching of $[Au(CN)_2]^-$ via oxidative electron transfer. At low temperatures (<129 K) electron transfer is absent resulting in $[Au(CN)_2]^-$ $S_1\rightarrow S_0$ emission. S_0, ground state; S_1, first excited state; T_1, first triplet state; NR, nonradiative decay; ET, electron transfer.

Electron Transfer Analysis. An analysis of this system was performed via Stern-Volmer and a Rehm-Weller to support the proposed electron transfer. First, a Stern-Volmer analysis was performed in order to examine the nature of $\mathbf{7}^{2+}$ quenching of $[Au(CN)_2]^-$, specifically to determine if the observed quenching is due

to electron transfer or resonance.[34] First, the ground state absorption spectra of the components were compared to the combined mixture. **Fig. 7** shows that the absorption spectrum of a mixture of $\mathbf{7}^{2+}$ and potassium dicyanoaurate is the simple sum of the two component absorption spectra. The lack of an additional absorption band in the mixed spectrum indicates that no ground state electronic interaction occurs between the two species. From this observation, we conclude that no static quenching occurs in this system.

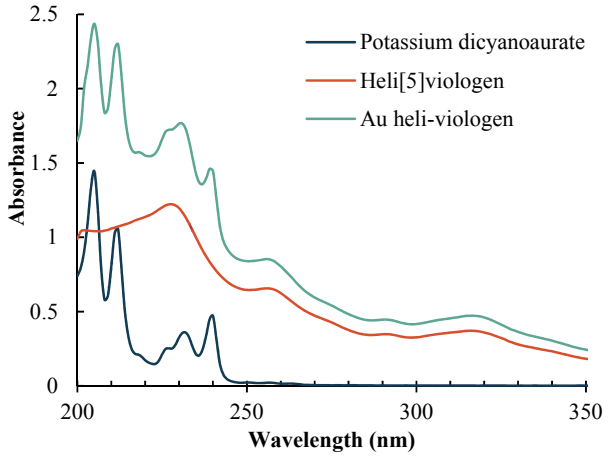

Fig. 7. Absorption spectra of potassium dicyanoaurate, heli[5]viologen, and Au heli-viologen in methanol (5 x 10^{-4} M).

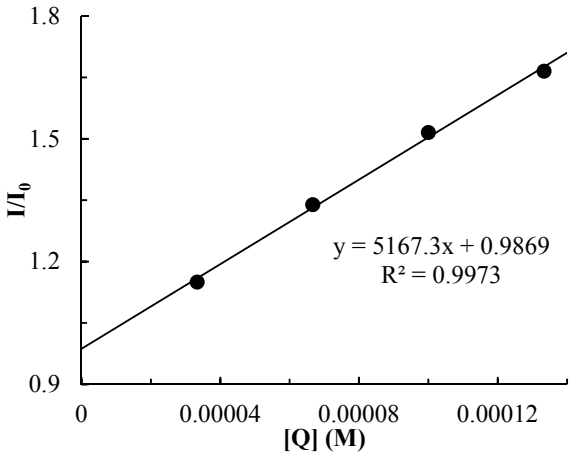

Fig. 8. Stern-Volmer plot for aqueous Au heli-viologen.

While our previous experiment indicates no ground-state quenching, we further investigated the possibility of quenching in the excited-state. The effect of $\mathbf{7}^{2+}$ as a dynamic quencher of $[Au(CN)_2]^-$ photoluminescence was investigated by measuring the photoluminescence of a series of $\mathbf{7}^{2+}$ /dicyanoaurate solutions. Luminescence intensity associated with $[Au(CN)_2]^-$ was observed to decrease as the concentration of $\mathbf{7}^{2+}$ was increased. Since we observe photoluminescence quenching upon addition of $\mathbf{7}^{2+}$, this data can be fit to the Stern-Volmer equation to further analyze the photophysical kinetics of the system. **Fig. 8** shows the Stern-Volmer plot constructed for this experiment. From this plot a K_{SV} value can be determined **(K_{SV} = 5170 M^{-1}).** The data show that quenching is observed for this system. This indicates that there is a significant interaction between gold dicyanoaurate species and $\mathbf{7}^{2+}$ during the photophysical excitation and relaxation process. This observation provides further support for our assignment of the emission band observed at 608 nm as a $[Au(CN)_2]^- \rightarrow \mathbf{7}^{2+}$ electron transfer.

The Rehm-Weller Equation[35] can be used to support the proposed electron transfer by determining whether the process is thermodynamically favorable.

$$\Delta G_{ET} = (E_{ox} - E_{red}) - E_s - e_o^2/\varepsilon_a$$

In the Rehm-Weller Equation shown above, ΔG_{ET} is the free energy change associated with the electron transfer process, E_{red} and E_{ox} are the reduction potential of the viologen $\mathbf{7}^{2+}$ acceptor and oxidation potential of the $[Au(CN)_2]_2^{2-}$ donor respectively, E_s represents the energy of the singlet state energy at 78 K (average of the lowest energy excitation band and highest energy emission band), and e_o^2/ε_a is taken as the attraction that the ion pair experiences.[12,36] We have calculated the E_{ox} (1.74 eV) via DFT by taking the difference in energy between an optimized structure of $[Au(CN)_2]_2^{-2}$ and $[Au(CN)_2]^-$. For the Au heli-viologen, ΔG_{ET} is therefore calculated as: ((1.74 + 0.22) - 2.32 - 0.15) = -0.51 eV, indicating the electron transfer is spontaneous. This calculated free energy change supports an electron transfer process as a feasible explanation for the observed quenching system.

Computational Modelling. DFT calculations were performed to interpret the photophysical changes and emission spectra of Au heli-viologen upon excitation. A neutral model of gold(I) dicyanide coordinated to $\mathbf{7}^{2+}$, shown in **Fig. 9**, was developed containing both $[Au(CN)_2]^-$ and $[Au(CN)_2]_2^{-2}$ subunits. Calculated ground state geometry parameters, Table S3 (ESI), are in good agreement with experimental values with short Au···Au distances supportive of aurophilic interactions. Calculations at the $[Au(CN)_2]_2^{-2}$ center accurately predict a short Au···Au distance of 3.435 Å compared to an experimental value of 3.310 Å. The close contact distance between the CN^- anion and the N^+ cation of the phenyl (3.155 Å) is slightly shorter than the experimental value of 3.216 Å. We attribute this shortened distance to the lack of surrounding $[Au(CN)_2]^-$ ions normally present. The loss of surrounding anions causes our model to overly rely on the central electron rich $[Au(CN)_2]_2^{-2}$ dimer to balance the cationic viologen ion.

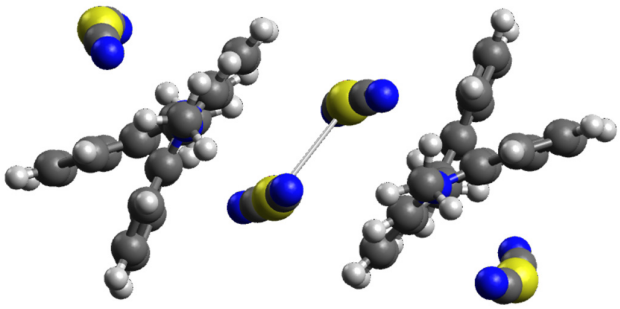

Fig. 9. DFT M06/CEP-31G(d) calculated ground state of $[Au(CN)_2]^-$ /$[Au(CN)_2]_2^{-2}$ coordinated 7^{2+}. Close Au···Au distance (3.435 Å) shown.

TD-DFT calculated UV-vis spectra, **Fig. S14** (ESI), show agreement of our model with the experimental UV-Vis results with both having strong absorption bands at energies higher than 500 nm. An excited state at 399 nm is predicted with a strong oscillator strength of 0.0132. This excited state energy aligns with our experimental luminescence excitation value of 400 nm. The highest contributing molecular orbital transition calculations performed for this excited state are shown in **Fig. 10 (**complete list of contributions summarized and illustrated in **Table S5** and **Fig. S15** (ESI)). TD-DFT calculations predict that two general types of electron transitions occur upon excitation at 399 nm. The first centers on the electron donating MOs (HOMO-9, and HOMO-11) which are primarily composed of the $\mathbf{7}^{+2}$ π* with minor contribution from the neighboring $[Au(CN)_2]^-$ anion. The electron accepting MO (LUMO) is composed of the $\mathbf{7}^{2+}$ π* and clearly represents a $\pi\rightarrow\pi$* transition. In the second case, the electron donating MO (HOMO) is exclusively composed of the dimerized $[Au(CN)_2]_2^{-2}$ subunit with no contribution from the neighboring $\mathbf{7}^{+2}$ cations. This molecular orbital calculated transition is clearly an electronic transfer and demonstrates the emissive quenching of $[Au(CN)_2]^-$ by the viologen in the solid state observed in the experimental photophysical data.

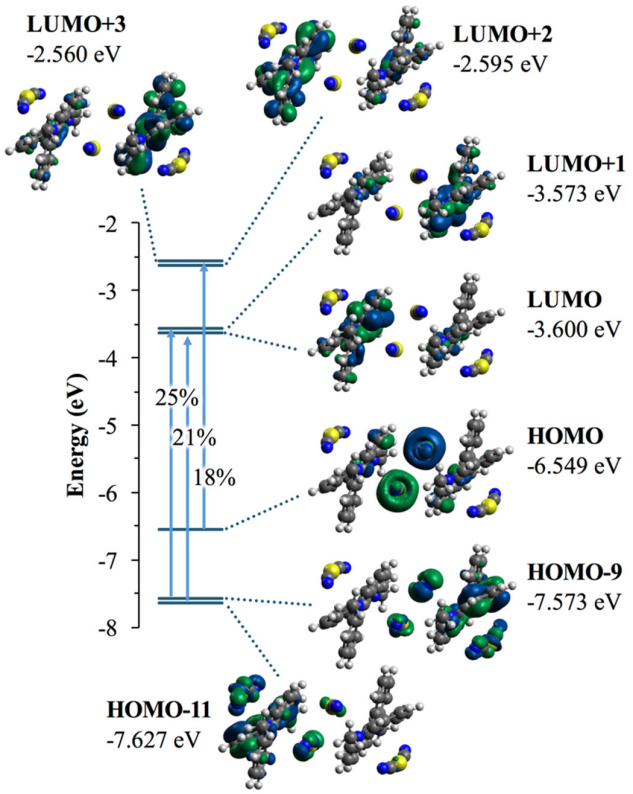

Fig. 10. TD-DFT M06/CEP-31G(d) energy diagram calculated for Au heli-viologen at 399 nm excitation for top 3 transitions. Transition percent contributions are noted.

Conclusions

Here we report for the first time the synthesis of a 2D network Au heli-viologen. The structure, characterized by single crystal X-ray diffraction, was found to consist of $[Au(CN)_2]^-$ dimers and monomers trapped within $\mathbf{7}^{2+}$ units. Photophysical studies show that at 298 K this complex emits at 580 nm via a triplet $\pi\rightarrow\pi$* transition localized to the $\mathbf{7}^{2+}$. Cooling to low temperatures results in a new emission band at 608 nm. Lifetime measurements and DFT calculations indicate that this new singlet band is the appearance of $[Au(CN)_2]_2^{-2}$ emission. The lack of this emission at temperatures higher than 129 K indicates that quenching occur from $\mathbf{7}^{2+}$. Stern-Volmer and Rehm-Weller analysis of this transition supports our assignment by revealing that quenching of $[Au(CN)_2]_2^{-2}$ by $\mathbf{7}^{2+}$ involves the transfer of an electron between ion pairs. Study of further 2D/3D networks involving better electron donors (such as dicyanoargentate coupled to MV^{2+}) will provide insight into the electron-transfer phenomenon investigated here.

Conflicts of interest

There are no conflicts of interest to declare.

Acknowledgements

The HHP group thanks the University of Maine Advanced Computing Group for their support and generous allocation of computing resources. MAO gratefully acknowledges support to his group's contributions by the Robert A. Welch Foundation (B-1542) and the US National Science Foundation (NSF -- CHE-1413641). MAO and EWR acknowledge NSF's MRI Program (CHE-1726652) for supporting the acquisition of the Rigaku XtaLAB Synergy-S X-ray diffractometer by the University of North Texas.

Notes and references

1 T. Nagamura, S. Muta and K. Shiratori, *Chem. Phys. Lett.*, 1995, **238**, 353–358.
2 T. Nagamura and K. Sakai, *J. Chem. Soc. Faraday Trans. 1 Phys. Chem. Condens. Phases*, 1988, **84**, 3529–3537.
3 T. Nagamura, *Pure Appl. Chem.*, 1996, **68**, 1449–1454.
4 D. Cummins, G. Boschloo, M. Ryan, D. Corr, S. N. Rao and D. Fitzmaurice, *J. Phys. Chem. B*, 2000, **104**, 11449–11459.
5 X. Zhang, E. L. Clennan, N. Arulsamy, R. Weber and J. Weber, *J. Org. Chem.*, 2016, **81**, 5474–5486.
6 A. S. Abouelwafa, V. Mereacre, T. S. Balaban, C. E. Anson and A. K. Powell, *CrystEngComm*, 2010, **12**, 94–99.
7 A. S. Abouelwafa, C. E. Anson, A. Hauser, H. H. Patterson, F. Baril-Robert, X. Li and A. K. Powell, *Inorg. Chem.*, 2012, **51**, 1294–1301.
8 D. L. Nelson and M. M. Cox, *Lehninger Principles of Biochemistry*, Macmillan, 5th edn., 2010.
9 A. G. Sharpe, *Acadmic Press London*.
10 D. Chasseau, P. Guionneau, M. Rahal, G. Bravic, J. Gaultier, L. Ducasse, M. Kurmoo and P. Day, *Synth. Met.*, 1995, **70**, 945–946.
11 D. B. Leznoff, B.-Y. Xue, R. J. Batchelor, F. W. B. Einstein and B. O. Patrick, *Inorg. Chem.*, 2001, **40**, 6026–6034.
12 X. Zhang, E. L. Clennan and N. Arulsamy, *Org. Lett.*, 2014, **16**, 4610–4613.
13 C. Bazzini, S. Brovelli, T. Caronna, C. Gambarotti, M. Giannone, P. Macchi, F. Meinardi, A. Mele, W. Panzeri, F. Recupero, A. Sironi and R. Tubino, *European J. Org. Chem.*,

2005, 1247–1257.
14 A. Irfan, M. Assiri and A. G. Al-Sehemi, *Org. Electron. physics, Mater. Appl.*, 2018, **57**, 211–220.
15 B. Spingler, S. Schnidrig, T. Todorova and F. Wild, *CrystEngComm*, 2012, **14**, 751–757.
16 R. O. Diffraction, 2017.
17 Rigaku Oxford Diffraction, 2017.
18 G. M. Sheldrick, *Acta Crystallogr. Sect. A Found. Adv.*, 2015, **71**, 3–8.
19 L. J. Bourhis, O. V. Dolomanov, R. J. Gildea, J. A. K. Howard and H. Puschmann, *Acta Crystallogr. Sect. A Found. Adv.*, 2015, **71**, 59–75.
20 O. V. Dolomanov, L. J. Bourhis, R. J. Gildea, J. A. K. Howard and H. Puschmann, *J. Appl. Crystallogr.*, 2009, **42**, 339–341.
21 A. L. Spek, *Acta Crystallogr. Sect. D Biol. Crystallogr.*, 2009, **65**, 148–155.
22 A. L. Spek, *Acta Crystallogr. Sect. C Struct. Chem.*, 2015, **71**, 9–18.
23 Frisch, M. J.; Trucks, G. W.; Schlegel, H. B.; Scuseria, G. E.; Robb, M. A.; Cheeseman, J. R.; Scalmani, G.; Barone, V.; Mennucci, B.; Petersson, G. A.; Nakatsuji, H.; Caricato, M.; Li, X.; Hratchian, H. P.; Izmaylov, A. F.; Bloino, J.; Zheng, G.; Sonnenberg, J. L.; Hada, M.; Ehara, M.; Toyota, K.; Fukuda, R.; Hasegawa, J.; Ishida, M.; Nakajima, T.; Honda, Y.; Kitao, O.; Nakai, H.; Vreven, T.; Montgomery, J. A.; Peralta, Jr., J. E.; Ogliaro, F.; Bearpark, M.; Heyd, J. J.; Brothers, E.; Kudin, K. N.; Staroverov, V. N.; Kobayashi, R.; Normand, J.; Raghavachari, K.; Rendell, A.; Burant, J. C.; Iyengar, S. S.; Tomasi, J.; Cossi, M.; Rega, N.; Millam, J. M.; Klene, M.; Knox, J. E.; Cross, J. B.; Bakken, V.; Adamo, C.; Jaramillo, J.; Gomperts, R.; Stratmann, R. E.; Yazyev, O.; Austin, A. J.; Cammi, R.; Pomelli, C.; Ochterski, J. W.; Martin, R. L.; Morokuma, K.; Zakrzewski, V. G.; Voth, G. A.; Salvador, P.; Dannenberg, J. J.; Dapprich, S.; Daniels, A. D.; Farkas, O.; Foresman, J. B.; Ortiz, J. V.; Cioslowski, J.; Fox, D. J. Gaussian 16, Revision B.01, Gaussian, Inc., Wallingford CT, **2016**.
24 Y. Zhao and D. G. Truhlar, *Theor. Chem. Acc.*, 2008, **120**, 215–241.
25 Y. Zhao and D. G. Truhlar, *Acc. Chem. Res.*, 2008, **41**, 157–167.
26 W. J. Stevens, M. Krauss, H. Basch and P. G. Jasien, *Can. J. Chem.*, 1992, **70**, 612–630.
27 T. R. Cundari and W. J. Stevens, *J. Chem. Phys.*, 1993, **98**, 5555–5565.
28 M. D. Hanwell, D. E. Curtis, D. C. Lonie, T. Vandermeersch, E. Zurek and G. R. Hutchison, *J. Cheminform.*, 2012, **4**, 17.
29 M. Stender, M. M. Olmstead, A. L. Balch, D. Rios and S. Attar, *Dalton Trans.*, 2003, 4282.
30 R. Galassi, M. M. Ghimire, B. M. Otten, S. Ricci, R. N. McDougald, R. M. Almotawa, D. Alhmoud, J. F. Ivy, A.-M. M. Rawashdeh, V. N. Nesterov, E. W. Reinheimer, L. M. Daniels, A. Burini and M. A. Omary, *Proc. Natl. Acad. Sci.*, 2017, 201700890.
31 D. Yang, Y. Jiao, L. Yang, Y. Chen, S. Mizoi, Y. Huang, X. Pu, Z. Lu, H. Sasabe and J. Kido, *J. Mater. Chem. A*, 2015, **3**, 17704–17712.
32 A. D. Nicholas, D. A. Welch, X. Li and H. H. Patterson, *Inorganica Chim. Acta*, 2018, **471**, 40–49.
33 X. Li and H. Patterson, *Materials (Basel).*, 2013, **6**, 2595–2611.
34 E. L. Clennan, X. Zhang and T. Petek, *Phosphorus. Sulfur. Silicon Relat. Elem.*, 2017, **192**, 222–226.
35 D. Rehm and A. Weller, *Isr. J. Chem.*, 1970, **8**, 259–271.
36 D. Parker, *Coord. Chem. Rev.*, 2000, **205**, 109–130.